Improved Synergetic Current Control for Grid-connected Microgrids and Distributed Generation Systems

A. Elnady, A. Noureldin, and A. A. Adam

***Abstract*—This paper presents the development of improved synergetic current control for the injected current of an inverter in the grid-connected microgrid and the distributed generation system (DGS). This paper introduces new formulas of the macro-variable functions for integral synergetic control (SC) and integral fast terminal SC, which both have an integral term to guarantee zero steady-state error. The proposed integral SC and integral fast terminal SC achieve a seamless performance such as the fast convergence, minimal overshoot, zero steady-state error, and chattering-free operation. To demonstrate the meritorious performance of the proposed scheme for injected current control, it is compared with the performance of a proportional-integral (PI) controller and advanced exponential sliding mode control (SMC). Finally, the practicality of the proposed scheme is justified by experimental results obtained through rapid control prototyping (RCP) using the dSPACE-SCALEXIO platform.**

***Index Terms*—Integral synergetic control (SC), current control, integral fast terminal SC, advanced exponential sliding mode control (SMC), proportional-integral (PI) control, microgrid, distributed generation system (DGS).**

I. Introduction

THE distributed generation systems (DGSs) become a new trend in electric power distribution systems because of the several merits associated with the existence of DGSs [1], [2]. The DGS is a group of dispersed energy resources (DESs) connected to the medium- and low-voltage power systems. These DESs can be conventional or unconventional energy resources such as diesel engines, microturbine-based generators, and renewable energy sources. Some of these energy resources require inverters for their energy processing [3], so inverters become the core components in the DGS or microgrid due to their vital role in processing the output current, power, voltage, and frequency. These inverters require an operational scheme to control their outputs based on the requirements of the DGS and microgrid.

The ultimate objective of DGS is to inject current and power into the distribution system and feed local loads according to their power requirements. This implies that the DGS should operate in a constant-current or constant-power mode, which is similar to the microgrid when it is connected to the main power grid [4]. The operation of microgrid in the grid-connected mode should be adjusted to enable the inverters to inject current and power into the main distribution system. Under this condition, the regulation of voltage and frequency is the responsibility of the main power grid [5].

This paper focuses on the current and power injected from the DGS and microgrid into the main power grid. Thus, the literature review focuses on different control techniques and schemes for current control along with different controllers related to the regulation of the injected current and power of the DGS. Reference [6] investigates some control schemes adopted to control the injected power of inverters in the DGS [6]. The voltage orientation control (VOC) is developed to control the power using two current loops (direct and quadrature current loops) through regular proportional-integral (PI) controllers [6]-[8]. However, the main drawback is that the utilization of PI controllers does not provide its best performance under different operation conditions. The first-order sliding mode control (SMC) is developed and coupled with power control to operate the DGS to regulate the injected power in the grid-connected mode [6], [9]-[11], but its main flaws are the chattering phenomenon and the moderate dynamic performance. The second-order SMC based on the super-twisting technique is developed to regulate the output power of the DGS to minimize the power chattering [12] and it provides slightly better results than the first-order SMC presented in [9]. The direct power control (DPC) scheme is adopted for the operation of DGSs, which provides a better performance with less chattering than SMC. Moreover, it produces a better dynamic performance compared with VOC, as proven in [6]. The adaptive control in the form of a single-perceptron-based PI controller is integrated with the DPC scheme to improve its transient performance with different power references [13]. The perfor-

Manuscript received: April 22, 2021; revised: September 24, 2021; accepted: February 2, 2022. Date of CrossCheck: February 2, 2022. Date of online publication: April 15, 2022.

This work was supported by the University of Sharjah (No. 20020403142 and No. 21020403178).

A. Elnady (corresponding anthor) and A. A. Adam are with Department of Electrical Engineering, University of Sharjah, Sharjah, United Arab Emirates, and A. Elnady is also with Department of Electrical and Computer Engineering, Royal Military College, Kingston, Canada (e-mail: ayelnady71@gmail.com; aismail@sharjah.ac.ae).

A. Noureldin is with Department of Electrical and Computer Engineering, Royal Military College, Kingston, Canada, and he is also with Department of Electrical and Computer Engineering, Queens University, Kingston, Canada (e-mail: Aboelmagd.Nourledin@rmc.ca).

DOI: 10.35833/MPCE.2021.000336

mance of adaptive control for injected power is much better than that of the regular PI controller for the DPC scheme. The predictive control scheme is combined with DPC in [14], [15]. The inaccuracy of the model and the uncertainties of the system parameters are overcome by the prediction of power and current as well as the online parameter of [14]. In [15], the predictive control is also adopted to alleviate the complexity of space vector modulation of the three-phase inverter, which is reflected in the reduction of harmonics. The power tracking performance using predictive control shows some oscillations [14] and a fast tracking performance [15].

The injected active power and reactive power are regulated in the constant-power or constant-current mode. The constant-power mode is realized through the precise power control along with its direct measurements, i.e., a regular DPC scheme. The constant-current mode is realized by regulating the corresponding direct and quadrature current loops.

The research in this paper belongs to the constant-current mode. Therefore, several important controllers of the current control loops for power adjustment are surveyed. A proportional-resonant (PR) controller is used for the current and power regulation of inverter-based DGSs [16]. It has a good current tracking performance, but it is sensitive to the frequency variation. The optimal control is implemented in the form of a linear quadratic regulator (LQR) to regulate the current of inverter coupled with the power grid through an LCL filter [17]. However, it is mathematically complicated because it is coupled with Kalman filter to improve the quality of estimating the system states. The predictive controller is also accompanied with the injected current of inverter in the DGS [18] to precisely regulate its output current even though this controller is sensitive to the uncertainties of system parameters. The nonlinear current control with feedback linearization is developed to achieve a unity power factor of its injected power [19]. An H_∞ controller is used to regulate the inverter to inject a sinusoidal current into the main power grid [20]. However, it has a relatively slow dynamic performance. The repetitive current controller is implemented in a parallel combination of resonant controllers with a high gain at harmonics [21]. Therefore, it can well reject disturbances at harmonic frequencies and consequently maintain the injected current and voltage at a high quality. The conventional synergetic control (SC) is integrated with the current loops in the *d-q* frame for the inverter connected to a photovoltaic (PV) system [22], where the manifold function is defined as the current error.

This paper presents the improved synergetic current control to regulate the injected current of inverter in the DGS or microgrid connected to the main power grid. The contributions of this paper are focused on the following points.

1) The steady-state performance of the macro-variable function is improved by replacing a differential term with an integral term, i.e., integral macro-variable function.

2) Two developed control techniques, i.e., integral SC and integral fast terminal SC, are implemented in a DGS or microgrid, which is a new application of SC.

3) The proposed integral SC and integral fast terminal SC, nonlinear control (advanced exponential SMC), and linear control (PI controller) are compared for the same application.

4) The practical implementation of the proposed scheme through rapid control prototyping (RCP) is conducted using the dSPACE-SCALEXIO platform.

The remainder of this paper is organized as follows. Section II details the model of DGS. Section III describes the proposed control schemes along with the mathematical formula. Section IV presents the simulation results. Section V details the results obtained with an experimental setup. Section VI summarizes the technical outcomes.

II. Model of DGS

The control scheme is proposed for a DGS or microgrid in the grid-connected mode. The parameters of this power system are listed in Table I. For the sake of simplicity, a DGS is considered in this paper. As shown in Fig. 1, this DGS connected to a distribution system contains a multilevel inverter, and some local loads are connected to the point of common coupling (PCC).

TABLE I
Parameters of Power System

Parameter	Value
Rated phase voltage V_{DS} (V)	110
Resistance of feeder R (Ω)	1
Inductance of feeder L (mH)	1.6
Impedance of load Z_L (Ω)	200+j21.98
Frequency of simulation (kHZ)	20
Carrier frequency for PD-PWM (kHZ)	2
DC voltage (V)	400
Inductance of inverter L_{filter} (mH)	20
Conductor of inverter C_{filter} (μF)	25
$V_{PCC,d}$ (V)	155
$V_{PCC,q}$ (V)	0

The system voltage is set to be 110 V, which is particularly chosen to match the simulation and experimental results.

The adopted inverter is a five-level diode-clamped inverter that minimizes the injected harmonics and eases its filter design. Therefore, the voltage of the inverter bus E is very close to a sinusoidal waveform. The adopted switching modulation is phase-disposition pulse-width modulation (PD-PWM), which perfectly fits the operation of this five-level inverter. The detailed operation and structure of the inverter topology as well as its switching modulation, operability, and control are detailed in [23].

The contribution of this paper is exemplified by the developed control law block in Fig. 1, whose input and output are the current error e and expected output voltage u, respectively. The output voltage u represents the required injected voltages E, and it is almost sinusoid because of the adopted topology of the inverter. In Fig. 1, V_{PCC} is the nominal voltage at PCC of the distribution system; I_{DG} is the current injected from the DGS; P and Q are the active and reactive power, respectively; I_d and I_q are the d- and q-axis injected currents from the DGS, respectively; the subscript ref represents the reference values; the subscripts a, b, and c represent phases a, b, and c, respectively; and the subscripts d and q represent the d- and q-axis values, respectively.

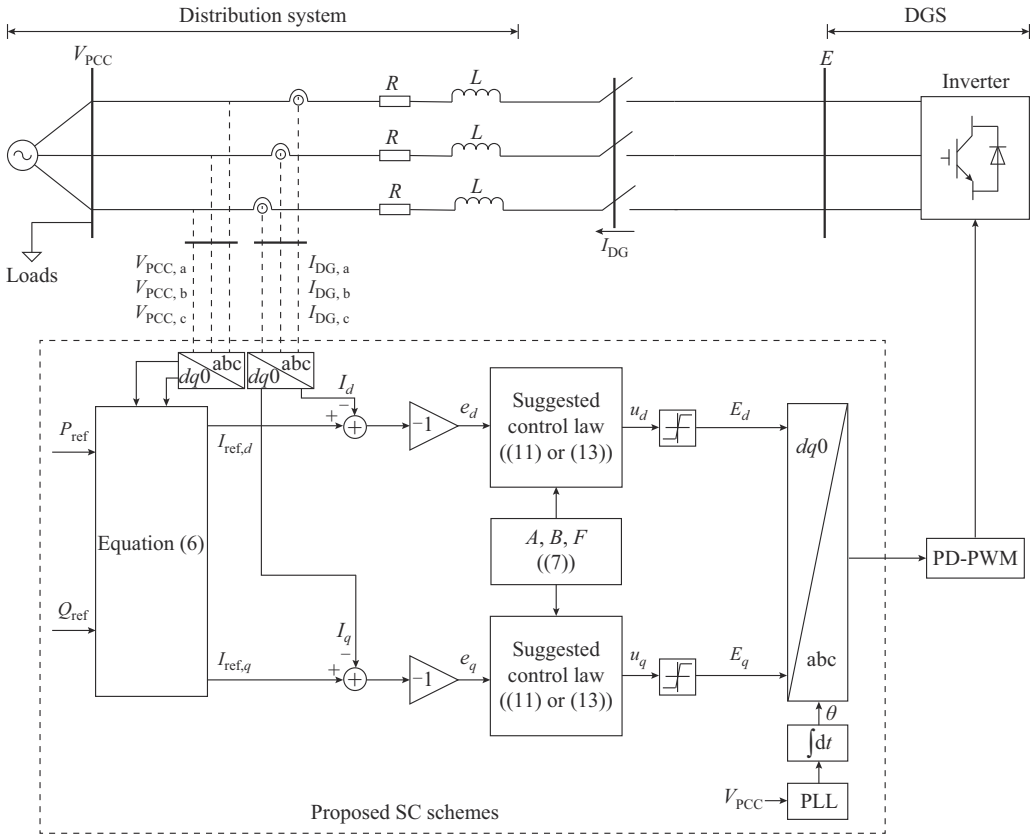

Fig. 1. Topology of power system with proposed SC schemes.

III. Proposed Control Schemes

This section presents the proposed control schemes and makes comparison between the proposed controller and other controllers.

A. Integral SC

SC is state space based nonlinear control for high-dimensional systems, which is first proposed in [24] and limited to some specific applications such as DC choppers [25], [26]. Recently, the conventional SC is applied to microgrid applications [22], [27]. SC is analogous to SMC, and it shares certain characteristics of SMC such as a reduction in the system order and intrinsic decoupling among system states. However, it outperforms SMC in terms of the reduced number of controller parameters, reduced chattering, and full controllability of the reaching mode. The main objective of the SC is to direct the system states to a certain manifold, i.e., sliding manifold. The macro-variable function is determined based on the system modeling and control objectives, and it is mainly a mathematical combination of state variables or state errors. The dynamic evolution of a macro-variable to the suggested manifold is defined as:

$$\begin{cases} \boldsymbol{T}\dot{\boldsymbol{\psi}}+\boldsymbol{\varphi}(\boldsymbol{\psi})=\boldsymbol{0} \\ \dot{\boldsymbol{\psi}}=\dfrac{\mathrm{d}\boldsymbol{\psi}}{\mathrm{d}\boldsymbol{x}}\dot{\boldsymbol{x}} \end{cases} \tag{1}$$

where $\boldsymbol{T}$ is a positive definite matrix defined as $\boldsymbol{T}=\begin{bmatrix} T_{Ip} & 0 \\ 0 & T_{Iq} \end{bmatrix}$, which determines the convergence rate of the macro-variable to the specific manifold, and T_{Ip} and T_{Iq} are the convergence rates of I_d and I_q, respectively; $\boldsymbol{x}$ is the error of state variables compared with their reference values; and $\boldsymbol{\varphi}(\boldsymbol{\psi})$ is the smooth function defined in [27]. The conventional macro-variable of SC is defined as [22], [24]-[27]:

$$\boldsymbol{\psi}(\boldsymbol{x})=\boldsymbol{x}+\dot{\boldsymbol{x}} \text{ or } \boldsymbol{\psi}(\boldsymbol{x})=\boldsymbol{x} \tag{2}$$

In [28] and [29], the terminal sliding manifold of SC is introduced and defined as:

$$\boldsymbol{\psi}(\boldsymbol{x})=\lambda\boldsymbol{x}^{\frac{a}{b}}+\dot{\boldsymbol{x}} \quad 0<\frac{a}{b}<1 \tag{3}$$

where λ is a real constant number; and parameters a and b are odd numbers satisfying $0<a/b<1$. The addition of a nonlinear term $\lambda\boldsymbol{x}^{a/b}$ to the conventional macro-variable improves the transient performance of the reaching mode and the robustness, as proven in [30], and the terminal SC becomes a necessary requirement, especially when the initial states are away from their suggested sliding manifold $\boldsymbol{\psi}(\boldsymbol{x})=\boldsymbol{0}$. Another version of the macro-variable formula with a better convergence is proposed and defined as [31]:

$$\boldsymbol{\psi}(\boldsymbol{x})=\boldsymbol{\lambda}_1\boldsymbol{x}^{\frac{a}{b}}+\boldsymbol{\lambda}_2\boldsymbol{x}+\dot{\boldsymbol{x}} \tag{4}$$

where $\boldsymbol{\lambda}_1$ and $\boldsymbol{\lambda}_2$ are the diagonal matrices with positive values defined as $\boldsymbol{\lambda}_1=\begin{bmatrix} \lambda_{1p} & 0 \\ 0 & \lambda_{1q} \end{bmatrix}$ and $\boldsymbol{\lambda}_2=\begin{bmatrix} \lambda_{2p} & 0 \\ 0 & \lambda_{2q} \end{bmatrix}$; and $\boldsymbol{x}$ can be commonly expressed as the error of state variables, i.e., $\boldsymbol{x}=\boldsymbol{e}$, and its formula has a fast convergence ($\dot{\boldsymbol{e}}=-\lambda_2\boldsymbol{e}$) when the error trajectory is away from the suggested manifold $\boldsymbol{\psi}(\boldsymbol{x})=\boldsymbol{0}$.

The injected current (or power) of the inverter is controlled to meet the requirements of the distribution system, where the microgrid or DGS is connected. The active power and reactive power in the *d-q* frame are expressed as:

$$\begin{bmatrix} P \\ Q \end{bmatrix} = \frac{3}{2}\begin{bmatrix} E_d & E_q \\ E_q & -E_d \end{bmatrix}\begin{bmatrix} I_d \\ I_q \end{bmatrix} \tag{5}$$

The current references $I_{\text{ref},d}$ and $I_{\text{ref},q}$ are obtained from the power references, which are expressed as:

$$\begin{bmatrix} I_{\text{ref},d} \\ I_{\text{ref},q} \end{bmatrix} = \frac{2}{3}\begin{bmatrix} E_d & E_q \\ E_q & -E_d \end{bmatrix}^{-1}\begin{bmatrix} P_{\text{ref}} \\ Q_{\text{ref}} \end{bmatrix} \tag{6}$$

The voltage-current state-space relationship is expressed as:

$$\begin{bmatrix} \dot{I}_d \\ \dot{I}_q \end{bmatrix} = \begin{bmatrix} -\frac{R}{L} & \omega \\ -\omega & -\frac{R}{L} \end{bmatrix}\begin{bmatrix} I_d \\ I_q \end{bmatrix} + \begin{bmatrix} \frac{1}{L} & 0 \\ 0 & \frac{1}{L} \end{bmatrix}\begin{bmatrix} E_d \\ E_q \end{bmatrix} + \begin{bmatrix} -\frac{1}{L} & 0 \\ 0 & -\frac{1}{L} \end{bmatrix}\begin{bmatrix} V_{\text{PCC},d} \\ V_{\text{PCC},q} \end{bmatrix} \Rightarrow \dot{\boldsymbol{x}}_I = \boldsymbol{A}\boldsymbol{x}_I + \boldsymbol{B}\boldsymbol{u} + \boldsymbol{F}\boldsymbol{d} \tag{7}$$

where $\boldsymbol{A} = \begin{bmatrix} -\frac{R}{L} & \omega \\ -\omega & -\frac{R}{L} \end{bmatrix}$; $\boldsymbol{B} = \begin{bmatrix} \frac{1}{L} & 0 \\ 0 & \frac{1}{L} \end{bmatrix}$; $\boldsymbol{F} = \begin{bmatrix} -\frac{1}{L} & 0 \\ 0 & -\frac{1}{L} \end{bmatrix}$; $\boldsymbol{u} = [E_d \quad E_q]^{\mathrm{T}}$; $\boldsymbol{d} = [V_{\text{PCC},d} \quad V_{\text{PCC},q}]^{\mathrm{T}}$; and $\boldsymbol{x}_I = [I_{\text{DG},d} \quad I_{\text{DG},q}]^{\mathrm{T}}$. The vector $\boldsymbol{d}$ represented by $V_{\text{PCC},d}$ and $V_{\text{PCC},q}$ is constant, and the error vector $\boldsymbol{e}$ is defined as:

$$\begin{cases} \boldsymbol{e} = [e_d \quad e_q]^{\mathrm{T}} \\ e_d = I_d - I_{\text{ref},d} \\ e_q = I_q - I_{\text{ref},q} \\ \dot{e}_d = \dot{I}_d, \dot{e}_q = \dot{I}_q \Rightarrow \dot{\boldsymbol{e}}_{dq} = \dot{\boldsymbol{x}}_I = \boldsymbol{A}\boldsymbol{x}_I + \boldsymbol{B}\boldsymbol{u} + \boldsymbol{F}\boldsymbol{d} \end{cases} \tag{8}$$

The error formula in (8) is substituted into a macro-variable function to derive the required control law. The main drawback of the conventional macro-variable function is its susceptibility to a nonzero steady-state error, as stated in [27] for the active and reactive power of a PV system and [32] for the current in a DC boost circuit.

In this paper, the idea of minimizing the steady-state error is deduced from the same concept applied to SMC, as stated in [33]. SC is not widely used for inverter control in the microgrid applications [22], [27]. As mentioned above, the conventional SC may be associated with some nonzero errors. Recently, the integral SC is formulated to directly control the injected power of inverters in the DGS [34]. In this paper, the integral SC is suggested to control the injected current of the inverter and eliminate the current errors, and its macro-variable function for the current errors in the *d-q* frame is expressed in a matrix form as:

$$\boldsymbol{\psi}(\boldsymbol{e}) = \boldsymbol{\lambda}_1 \boldsymbol{e} + \boldsymbol{\lambda}_2 \int \boldsymbol{e}\mathrm{d}\boldsymbol{t} \tag{9}$$

where $\int \boldsymbol{e}\mathrm{d}\boldsymbol{t} = \left[\int e_d \mathrm{d}t \quad \int e_q \mathrm{d}t\right]^{\mathrm{T}}$. This formula is then substituted into the dynamic evolution function of (1), which yields.

$$\boldsymbol{T}(\boldsymbol{\lambda}_1 \dot{\boldsymbol{e}} + \boldsymbol{\lambda}_2 \boldsymbol{e}) + \boldsymbol{\lambda}_1 \boldsymbol{e} + \boldsymbol{\lambda}_2 \int \boldsymbol{e}\mathrm{d}\boldsymbol{t} = \boldsymbol{0} \Rightarrow$$

$$\boldsymbol{T}\boldsymbol{\lambda}_1 \dot{\boldsymbol{e}} + (\boldsymbol{T}\boldsymbol{\lambda}_2 + \boldsymbol{\lambda}_1)\boldsymbol{e} + \boldsymbol{\lambda}_2 \int \boldsymbol{e}\mathrm{d}\boldsymbol{t} = \boldsymbol{0} \tag{10}$$

The control law is deduced in (11), which gives the required injected voltages of the inverter, i.e., $\boldsymbol{u} = [E_d \quad E_q]^{\mathrm{T}}$.

$$\boldsymbol{T}\boldsymbol{\lambda}_1 \dot{\boldsymbol{e}} + (\boldsymbol{T}\boldsymbol{\lambda}_2 + \boldsymbol{\lambda}_1)\boldsymbol{e} + \boldsymbol{\lambda}_2 \int \boldsymbol{e}\mathrm{d}\boldsymbol{t} = \boldsymbol{0} \Rightarrow$$

$$(\boldsymbol{T}\boldsymbol{\lambda}_1)^{-1}\left[-(\boldsymbol{T}\boldsymbol{\lambda}_2 + \boldsymbol{\lambda}_1)\boldsymbol{e} - \boldsymbol{\lambda}_2 \int \boldsymbol{e}\,\mathrm{d}\boldsymbol{t}\right] = \dot{\boldsymbol{e}} \tag{11}$$

where $\dot{\boldsymbol{e}} = \dot{\boldsymbol{x}}_I = \boldsymbol{A}\boldsymbol{x}_I + \boldsymbol{B}\boldsymbol{u} + \boldsymbol{F}\boldsymbol{d} \Rightarrow \boldsymbol{B}\boldsymbol{u} = -(\boldsymbol{T}\boldsymbol{\lambda}_1)^{-1}\left[(\boldsymbol{T}\boldsymbol{\lambda}_2 + \boldsymbol{\lambda}_1)\boldsymbol{e} + \boldsymbol{\lambda}_2 \int \boldsymbol{e}\mathrm{d}\boldsymbol{t}\right] - \boldsymbol{A}\boldsymbol{x}_I - \boldsymbol{F}\boldsymbol{d} \Rightarrow \boldsymbol{u} = -\boldsymbol{B}^{-1}\left\{(\boldsymbol{T}\boldsymbol{\lambda}_1)^{-1}\left[(\boldsymbol{T}\boldsymbol{\lambda}_2 + \boldsymbol{\lambda}_1)\boldsymbol{e} + \boldsymbol{\lambda}_2 \int \boldsymbol{e}\mathrm{d}\boldsymbol{t}\right] + \boldsymbol{A}\boldsymbol{x}_I + \boldsymbol{F}\boldsymbol{d}\right\}$.

The voltages are injected to make the output currents I_d and I_q follow their references. The stability of the proposed integral SC is illustrated in Appendix A Section A.

B. Integral fast Terminal SC

The terminal SC greatly forces the system states to converge to zero in a finite time [28]-[30] and consequently reduces its reaching time. The terminal SC in [28]-[30] is improved by the proposed fast terminal SC in [35]. This improvement is achieved by adding an error term to the manifold function to guarantee finite-time convergence to the desired manifold. As proven in [34] and [35], the fast terminal SC has a faster transient performance than the terminal SC. In this paper, the proposed macro-variable function of integral fast terminal SC is expressed as:

$$\boldsymbol{\psi}(\boldsymbol{e}) = \boldsymbol{\lambda}_1 \boldsymbol{e}^{\frac{a}{b}} + \boldsymbol{\lambda}_2 \boldsymbol{e} + \boldsymbol{\lambda}_3 \int \boldsymbol{e}\mathrm{d}\boldsymbol{t} \tag{12}$$

where $\boldsymbol{\lambda}_3 = \begin{bmatrix} \lambda_{3p} & 0 \\ 0 & \lambda_{3q} \end{bmatrix}$ is a positive definite matrix.

A stability analysis of (12) is detailed in Appendix A Section B. The control law is expressed as (13), which produces the reference value of the injected voltages $\boldsymbol{u}$.

$$\boldsymbol{T}\dot{\boldsymbol{\psi}} + \boldsymbol{\psi} = \boldsymbol{T}\boldsymbol{\lambda}_1 \frac{\mathrm{d}}{\mathrm{d}\boldsymbol{t}}\boldsymbol{e}^{\frac{a}{b}} + \boldsymbol{T}\boldsymbol{\lambda}_2 \dot{\boldsymbol{e}} + \boldsymbol{T}\boldsymbol{\lambda}_3 \boldsymbol{e} + \boldsymbol{\lambda}_1 \boldsymbol{e}^{\frac{a}{b}} + \boldsymbol{\lambda}_2 \boldsymbol{e} + \boldsymbol{\lambda}_3 \int \boldsymbol{e}\,\mathrm{d}\boldsymbol{t} = \boldsymbol{0} \Rightarrow$$

$$\dot{\boldsymbol{e}} = (\boldsymbol{T}\boldsymbol{\lambda}_2)^{-1}\left[-\left(\boldsymbol{T}\boldsymbol{\lambda}_1 \frac{\mathrm{d}}{\mathrm{d}\boldsymbol{t}} + \boldsymbol{\lambda}_1\right)\boldsymbol{e}^{\frac{a}{b}} - (\boldsymbol{T}\boldsymbol{\lambda}_3 + \boldsymbol{\lambda}_2)\,\boldsymbol{e} - \boldsymbol{\lambda}_3 \int \boldsymbol{e}\mathrm{d}\boldsymbol{t}\right] \tag{13}$$

where $\dot{\boldsymbol{e}} = \dot{\boldsymbol{x}}_I = \boldsymbol{A}\boldsymbol{x}_I + \boldsymbol{B}\boldsymbol{u} + \boldsymbol{F}\boldsymbol{d} \Rightarrow \boldsymbol{B}\boldsymbol{u} = (\boldsymbol{T}\boldsymbol{\lambda}_2)^{-1}\left[-\left(\boldsymbol{T}\boldsymbol{\lambda}_1 \frac{\mathrm{d}}{\mathrm{d}\boldsymbol{t}} + \boldsymbol{\lambda}_1\right)\boldsymbol{e}^{\frac{a}{b}} - (\boldsymbol{T}\boldsymbol{\lambda}_3 + \boldsymbol{\lambda}_2)\boldsymbol{e} - \boldsymbol{\lambda}_3 \int \boldsymbol{e}\mathrm{d}\boldsymbol{t}\right] - \boldsymbol{A}\boldsymbol{x}_I - \boldsymbol{F}\boldsymbol{d} \Rightarrow \boldsymbol{u} = -\boldsymbol{B}^{-1}\left\{(\boldsymbol{T}\boldsymbol{\lambda}_2)^{-1}\left[\left(\boldsymbol{T}\boldsymbol{\lambda}_1 \frac{\mathrm{d}}{\mathrm{d}\boldsymbol{t}} + \boldsymbol{\lambda}_1\right)\boldsymbol{e}^{\frac{a}{b}} + (\boldsymbol{T}\boldsymbol{\lambda}_3 + \boldsymbol{\lambda}_2)\boldsymbol{e} + \boldsymbol{\lambda}_3 \int \boldsymbol{e}\mathrm{d}\boldsymbol{t}\right] + \boldsymbol{A}\boldsymbol{x}_I + \boldsymbol{F}\boldsymbol{d}\right\}$.

C. Power-rate Exponential SMC

This subsection compares the proposed control scheme with a strong robust nonlinear control, which is the advanced power-rate exponential SMC detailed in [36]. The SMC presented in this paper is based on the concept of exponential SMC, of which the control law is defined by two

terms as [37]:

$$u = u_{eq} + u_{discrete} \tag{14}$$

where $u_{discrete}$ and u_{eq} are the discrete and equivalent terms, respectively.

The discrete term $u_{discrete}$ and its sliding manifold are defined in [36] for each state variable as:

$$\begin{cases} u_{discrete} = \dfrac{-k}{\delta_0 + (1-\delta_0)e^{-\alpha|s|^{\rho}}}\operatorname{sign}(s) \\ s = \lambda e + \dfrac{\mathrm{d}}{\mathrm{d}t}e \end{cases} \tag{15}$$

where α, ρ, δ_0, λ, and k are strictly positive, and $\delta_0 < 1$. The value of $u_{discrete}$ ranges from almost $-k/\delta_0$ with large s to almost $-k$ with small s. The stability of the advanced exponential SMC is detailed in [36] and [37]. The discrete term is modified by multiplying a power-rate term $|s|^{\mu}$ to the discrete input $u_{discrete}$ in (15), and the constant μ is a positive real number less than one [36]. The employed discrete term is expressed as:

$$u_{discrete} = \frac{-k_1|s|^{\mu}}{\delta_0 + (1-\delta_0)e^{-\alpha|s|^{\rho}}}\tanh(k_2 s) \tag{16}$$

where k_1 and k_2 are the real positive numbers.

The sliding surface $\boldsymbol{s}$ for all state variables $\boldsymbol{e}$ is defined as $\boldsymbol{s} = \boldsymbol{\lambda}_1'\boldsymbol{e} + \boldsymbol{\lambda}_2'\int \boldsymbol{e}\mathrm{d}\boldsymbol{t}$, where $\boldsymbol{\lambda}_1'$ and $\boldsymbol{\lambda}_2'$ are the real positive diagonal matrices.

The stability of the discrete term in (16) is thoroughly documented in [36]. The performance of power-rate exponential SMC is faster than that of conventional exponential SMC in terms of the time required for its reaching mode.

The vector of equivalent term $\boldsymbol{u}_{eq}$ is derived from Lyapunov equation, which is expressed as:

$$\begin{aligned} &\boldsymbol{V}(\boldsymbol{s}) = \frac{1}{2}\boldsymbol{s}^{\mathrm{T}}\boldsymbol{s},\ \dot{\boldsymbol{V}}(\boldsymbol{s}) = \frac{\mathrm{d}\boldsymbol{V}(\boldsymbol{s})}{\mathrm{d}\boldsymbol{s}}\frac{\mathrm{d}\boldsymbol{s}}{\mathrm{d}\boldsymbol{t}} = \boldsymbol{s}^{\mathrm{T}}\boldsymbol{s} \le \boldsymbol{0} \Rightarrow \\ &\dot{\boldsymbol{s}} = \boldsymbol{\lambda}_1'\dot{\boldsymbol{e}} + \boldsymbol{\lambda}_2'\boldsymbol{e} = \boldsymbol{0},\ e_d = I_{\mathrm{ref},d} - I_d, e_q = I_{\mathrm{ref},q} - I_q \Rightarrow \\ &\dot{\boldsymbol{e}} = -\dot{\boldsymbol{x}}_1 \Rightarrow \dot{\boldsymbol{s}} = -\boldsymbol{\lambda}_1'(\boldsymbol{A}\boldsymbol{x}_1 + \boldsymbol{B}\boldsymbol{u}_{eq} + \boldsymbol{F}\boldsymbol{d}) + \boldsymbol{\lambda}_2'\boldsymbol{e} = \boldsymbol{0} \Rightarrow \\ &\boldsymbol{u}_{eq} = -(\boldsymbol{\lambda}_1'\boldsymbol{B})^{-1}(\boldsymbol{A}\boldsymbol{x}_1 + \boldsymbol{F}\boldsymbol{d} - \boldsymbol{\lambda}_2'\boldsymbol{e}) \end{aligned} \tag{17}$$

The discrete and equivalent terms are mathematically defined in (16) and (17), respectively. The final control law for all state variables in the vector from is defined as:

$$\boldsymbol{u} = \frac{-\boldsymbol{k}_1|\boldsymbol{s}|^{\mu}}{\boldsymbol{\delta}_0 + (1-\boldsymbol{\delta}_0)e^{-\alpha|\boldsymbol{s}|^{\rho}}}\tanh(\boldsymbol{k}_2\boldsymbol{s})(\boldsymbol{\lambda}_1'\boldsymbol{B})^{-1}(\boldsymbol{A}\boldsymbol{x}_1 + \boldsymbol{F}\boldsymbol{d} - \boldsymbol{\lambda}_2'\boldsymbol{e}) \tag{18}$$

Eventually, the control law in (18) can be adopted to produce the required injected voltages of inverter $\boldsymbol{u} = [E_d \quad E_q]^{\mathrm{T}}$.

D. PI-controller-based Current Control

A regular PI controller is the most commonly used because it does not require any state-space formulation or power system modeling. However, the PI controller cannot directly replace the control block of SC in Fig. 1. Thus, to incorporate PI controllers, the scheme in Fig. 2 replaces the entire control scheme in Fig. 1 and it has already been deduced from the model given in (7). The rest of the power system in Fig. 1 remains the same.

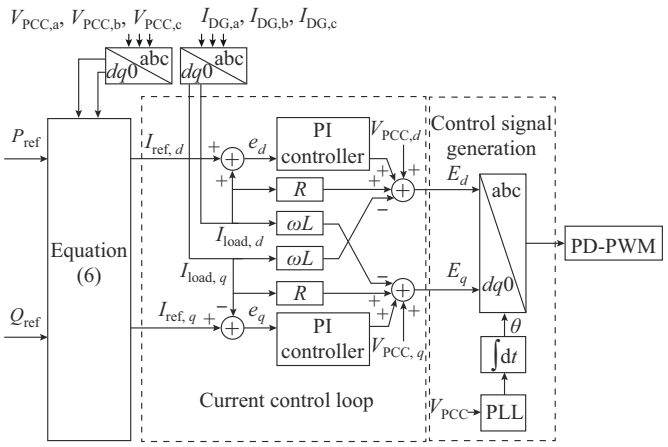

Fig. 2. PI-controller-based control scheme.

IV. Simulation Results

This section is divided into six different subsections, which present the simulation results with different controllers and the utilization of the suggested control scheme with two inverters in the studied system. The simulations are conducted under the same conditions with the same power references and loads as listed in Table I for all presented controllers. The values of the controller parameters are selected by trials and errors. Many trials are conducted to achieve the best performance for each controller presented in these subsections.

A. Simulation Results for PI-controller-based Current Control

In this subsection, the control scheme in Fig. 2 is adopted. The parameters of PI controllers are set as $k_P = 0.00625$ and $k_I = 0.855$ for the direct current loop and $k_P = 0.0125$ and $k_I = 0.3375$ for the quadrature current loop. The power tracking performances of PI controller and power-rate exponential SMC are shown in Fig. 3, where Exp-SMC represents power-rate exponential SMC, PI represents PI controller, and Ref represents the reference signals. It can be observed that a regular PI controller does not provide its best performance under different operation conditions. Therefore, the transient performance and steady-state performance in terms of overshoot and error change from one operation to another.

B. Simulation Results for Power-rate Exponential SMC

In this subsection, the derived control law in (18) is adopted. This derived control law is used to produce the control signal required to operate the switching modulation of the adopted inverter, i.e., PD-PWM. The parameters of this controller for the best performance are listed in Table II. As shown in Fig. 3, the power tracking performance of power-rate exponential SMC shows a drastic improvement in the transient performance compared with the PI controller, and the integral sliding manifold helps minimize the steady-state error. Further, the chattering problem is drastically reduced by using power-rate exponential SMC, as expected and proven in [36], [37].

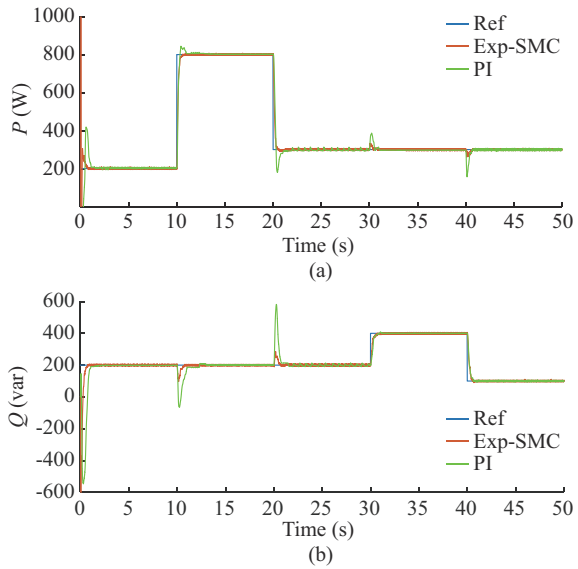

Fig. 3. Power tracking performances of PI controller and power-rate exponential SMC. (a) Active power. (b) Reactive power.

TABLE II
PARAMETERS OF POWER-RATE EXPONENTIAL SMC

d-axis parameter	*q*-axis parameter
$\lambda_1'=0.00125$	$\lambda_1'=0.00125$
$\lambda_2'=0.63$	$\lambda_2'=1.54$
$k_1=250$	$k_1=350$
$k_2=0.01$	$k_2=0.01$
$\delta_0=0.05$	$\delta_0=0.05$
$\mu=0.95$	$\mu=0.97$
$\rho=0.25$	$\rho=0.25$
$\alpha=0.04$	$\alpha=0.04$

C. Simulation Results for Integral SC

The integral SC is presented in Section III along with its control law in (11). The parameters of this control scheme are listed in Table III. As shown in Fig. 4, the power tracking performance of integral SC is very close to that of power-rate exponential SMC in terms of the 1st overshoot and steady-state error, but the suggested integral SC is slightly faster than SMC.

TABLE III
PARAMETERS FOR INTEGRAL SC

d-axis parameter	*q*-axis parameter
$\lambda_{1p}=1$	$\lambda_{1q}=1.5$
$\lambda_{2p}=2.5$	$\lambda_{2q}=1$
$T_p=0.000065$	$T_q=0.0001$

At the instants of transition for any power reference, the direction of the power spike for SC is opposite to that for SMC because of the error definition and its sign. The power-rate exponential SMC defines the current reference minus the current feedback as the current error, as shown in (17), whereas the integral SC defines the current feedback minus the current reference as the current error, as shown in (8). This justifies the opposite direction of the power spikes (at $t=10$, 20, 30, and 40 s), as shown in Fig. 4.

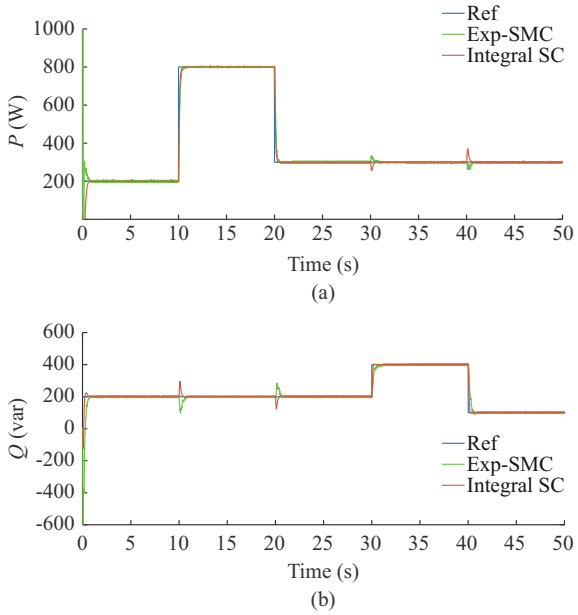

Fig. 4. Power tracking performances of power-rate exponential SMC and integral SC. (a) Active power. (b) Reactive power.

The advantage of integral SC is exemplified in its simplicity compared with the proposed SMC, as clarified by the number of tuned controller parameters shown in Tables II and III. Further, it is almost chattering-free compared with the proposed reduced-chattering SMC in this paper.

D. Simulation Results for Integral Fast Terminal SC

The control law of integral fast terminal SC is presented in Section III. The parameters of the control scheme shown in Fig. 1 are listed in Table IV. The current tracking performance of integral fast terminal SC is illustrated in Fig. 5(a) and (b), while the power tracking performance of integral fast terminal SC is depicted in Fig. 5(c) and (d) in comparison with that of the integral SC.

TABLE IV
PARAMETERS OF INTEGRAL FAST TERMINAL SC

d-axis parameter	*q*-axis parameter
$\lambda_{1p}=1$	$\lambda_{1q}=1$
$\lambda_{2p}=2.5$	$\lambda_{2q}=1$
$T_p=0.000085$	$T_q=0.0001$
$\lambda_{3p}=5$	$\lambda_{3q}=5$
$a=7$	$a=7$
$b=9$	$b=9$

The intrinsic decoupling between the active power and reactive power is clarified when the active power and reactive power change at $t=10$, 20, 30, and 40 s. The power performance is obtained from the current loop, which provides a seamless performance for I_d and I_q, as shown in Fig. 5(a) and (b).

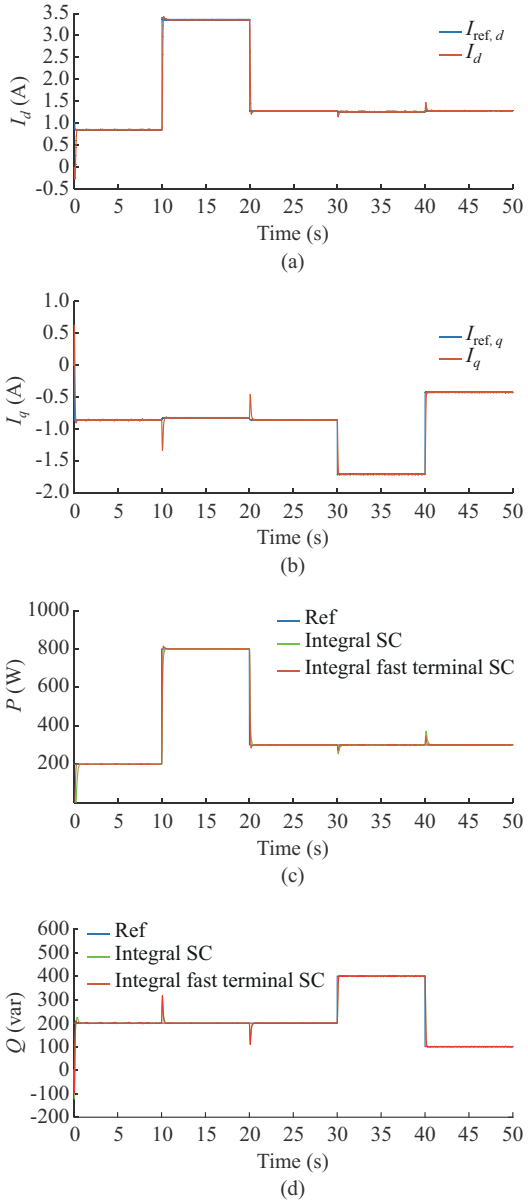

Fig. 5. Currents and power tracking performances of integral fast terminal SC and integral SC. (a) *d*-axis currents. (b) *q*-axis currents. (c) Active power. (d) Reactive power.

E. Comparative Theoretical Analysis of Different Controllers

The merits of integral fast terminal SC have been already articulated in terms of its speed and intrinsic decoupling between system states, as shown in Fig. 5. The transient power tracking performances of the proposed integral fast terminal SC compared with other controllers are illustrated in Fig. 6. A quantitative comparative analysis of the waveforms in Fig. 6 is presented in Table V. It is worth mentioning that the following conclusions can be drawn from the comparative analysis.

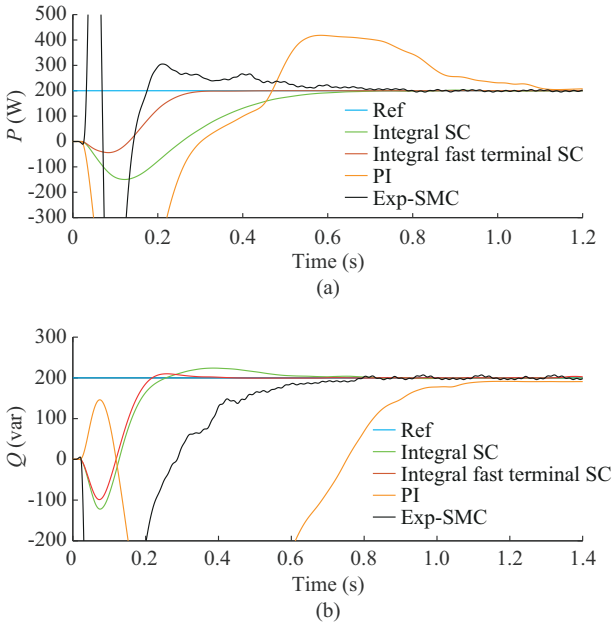

Fig. 6. Transient performances of integral fast terminal SC, integral SC, power-rate exponential SMC, and PI controller. (a) Active power. (b) Reactive power.

1) The power-rate exponential SMC is much better than the PI controller from the overshoot perspective. More importantly, the chattering of the proposed SMC is minimal, as illustrated in Fig. 3(a) and (b), and both controllers have almost zero steady-state error.

2) The integral SC has an advantage over the proposed SMC in terms of the overshoot, settling time, and chattering, as illustrated in Fig. 4.

3) The integral fast terminal SC is slightly faster than integral SC, which means that the system states reach their sliding trajectory faster than integral SC, and both controllers have almost zero error, as depicted in Fig. 6(a) and (b) for the active power and reactive power, respectively.

TABLE V
THEORETICAL QUANTITATIVE COMPARISON OF INTEGRAL FAST TERMINAL SC, INTEGRAL SC, AND POWER-RATE EXPONENTIAL SMC

Performance	Controller	The 1st overshoot (%)	Transient time (s)	Error	Chattering
Active power	Integral fast terminal SC	0	0.3	0	Free
	Integral SC	0	0.6	0	Free
	Power-rate exponential SMC	50	0.8	0	Small
Reactive power	Integral fast terminal SC	5	0.4	0	Free
	Integral SC	15	0.8	0	Free
	Power-rate exponential SMC	0	1.0	0	Small

F. Control Scheme for Parallel Inverters

The proposed SC scheme in Fig. 1 is modular because it is separately implemented on each inverter in the same DGS or microgrid. Each inverter should have its own control scheme and parameters. Based on the power system in Fig. 1, another inverter with its own control scheme is added in parallel to the first inverter, such that both inverters are connected in parallel at the PCC in Fig. 1. The injected currents I_{d1}, I_{d2}, I_{q1}, I_{q2} with their references $I_{\text{ref},d1}$, $I_{\text{ref},d2}$, $I_{\text{ref},q1}$, $I_{\text{ref},q2}$ for both inverters are shown in Fig. 7(a) and (b) for the d- and q-axis currents, respectively. The generated active and reactive power P_1, P_2, Q_1, Q_2 with their references $P_{\text{ref},1}$, $P_{\text{ref},2}$, $Q_{\text{ref},1}$, $Q_{\text{ref},2}$ of both inverters are shown in Fig. 7(c) and (d), respectively.

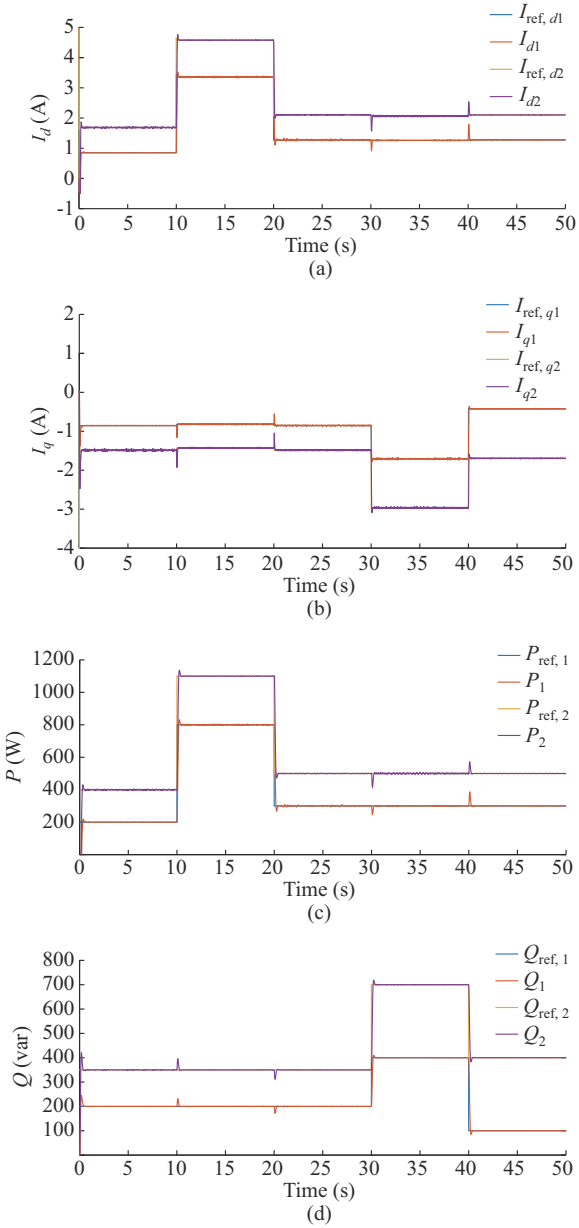

Fig. 7. Currents and power tracking performances for two parallel inverters. (a) d-axis currents. (b) q-axis currents. (c) Active power. (d) Reactive power.

The tracking performance in Fig. 7 is very similar to that in Fig. 5, indicating that the operation of the proposed SC schemes does not degrade with the parallel operation of the inverters. The circulating current is minimal because each inverter is operated in a constant-current mode.

V. Experimental Results

This section presents the experimental results for the controllers mentioned in Section IV. This section contains three subsections detailing the experimental setup along with the results for all different controllers and a comparative analysis among them.

A. Experimental Setup

The experimental prototype is similar to the DGS presented in Fig. 1, where the SC scheme is implemented on the dSPACE platform to realize RCP. The adopted experimental setup is given in Appendix B Fig. B1, which shows the adopted inverter topology, the passive filter, the tie feeder, the loads, the transformer connected to power grid, and the dSPACE platform along with its interface circuits. The parameters of the experimental setup are given in Table I, except that the sampling frequency is 10 kHz, the carrier frequency for PD-PWM is 1.25 kHz (avoiding possible overruns), and the transition of a power reference is conducted every 8 s. The RCP is implemented such that the proposed control scheme in Fig. 1 is executed on the dSPACE platform using Simulink. Then, the dSPACE platform generates control signals, which are received by the switching modulation circuit PD-PWM located outside the dSPACE. The power is calculated in the dSPACE and dispatched as an attenuated analog voltage signal to an oscilloscope with a channel setting of 100 W/div or 100 var/div to present the power tracking performance of different controllers.

B. Experimental Results for Different Controllers

In this subsection, the experimental results are presented for different controllers.

1) PI Controller

The control scheme shown in Fig. 2 is executed on the dSPACE platform. The performance of PI controllers whose parameters are given in Section IV is shown in Fig. 8(a) and (b) for the active power and reactive power, respectively, with their power references. The main features of the PI-controller-based control scheme are summarized as follows.

1) There is no consistency in its performance during different transitions.

2) The overshoot is the minimum, as shown at $t = 24$ s and $t = 32$ s in Fig. 8(b).

3) The coupling between the active power loop and the reactive power loop is considerable, as shown in the power transitions at $t = 8$ s and $t = 16$ s in Fig. 8(b).

2) Power-rate Exponential SMC

The power-rate exponential SMC is applied to the dSPACE platform. The controller parameters are similar to those listed in Table II. As shown in Fig. 8, the performance of power-rate exponential SMC is drastically improved compared with that of the PI controller.

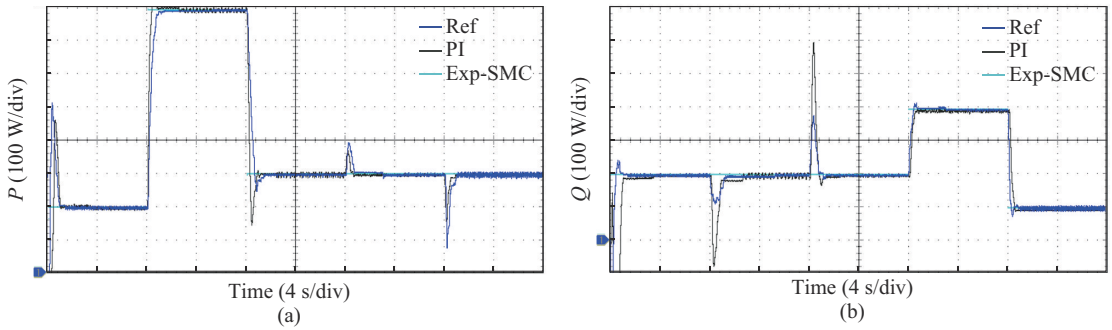

Fig. 8. Experimental results for power-rate exponential SMC and PI controller. (a) Active power. (b) Reactive power.

3) Proposed SCs

The integral SC and integral fast terminal SC in Fig. 1 along with their control laws in (11) and (13) are carried out on the dSPACE platform, respectively. The power tracking performances of integral SC and integral fast terminal SC are shown in Figs. 9 and 10, respectively.

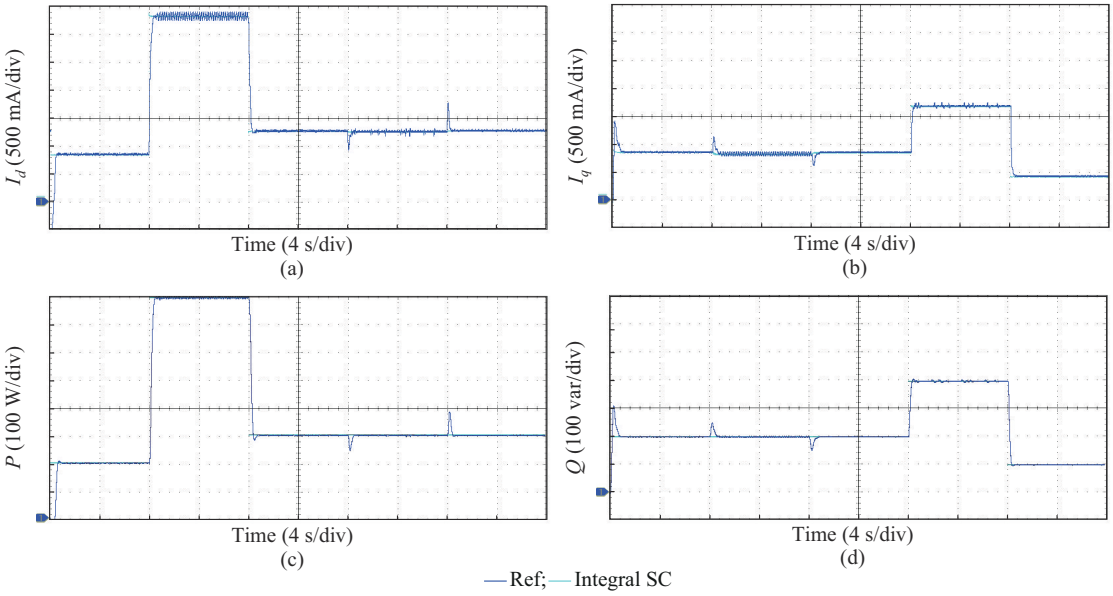

Fig. 9. Experimental results for current and power tracking of integral SC. (a) *d*-axis currents. (b) *q*-axis currents. (c) Active power. (d) Reactive power.

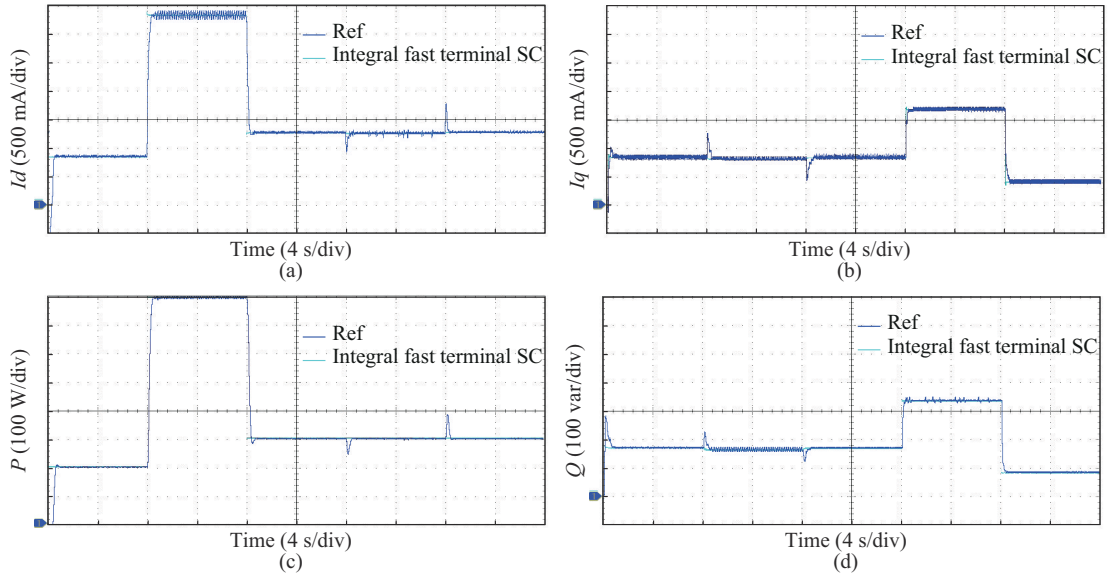

Fig. 10. Experimental results for current and power tracking of integral fast terminal SC. (a) *d*-axis currents. (b) *q*-axis currents. (c) Active power.(d) Reactive power.

The effects of integral SC on the *d*- and *q*-axis currents are shown in Fig. 9(a) and (b), respectively. The accurate current performance is reflected in the power tracking performance in Fig. 9(c) and (d) for active power and reactive power, respectively.

Similarly, the advantageous performance of integral fast terminal SC is illustrated in Fig. 10, where the system states reach the sliding manifold, as defined in (12), slightly faster than integral SC. The fast performance of integral fast terminal SC is quantified by certain indices, as explained in the Section V-C.

The current tracking performance of integral fast terminal SC is depicted in Fig. 10(a) and (b) for the *d*- and *q*-axis currents, respectively. The power tracking performance of integral fast terminal SC is shown in Fig. 10(c) and (d) for the active power and reactive power, respectively.

C. Comparative Experimental Analysis Among Different Controllers

A comparison between the suggested SCs, i.e., integral SC and integral fast terminal SC, and the power-rate exponential SMC is shown in Fig. 11(a) and (b) for the active power and reactive power, respectively. For an accurate comparison, the performance of all controllers in Fig. 11 is numerically quantified in Table VI.

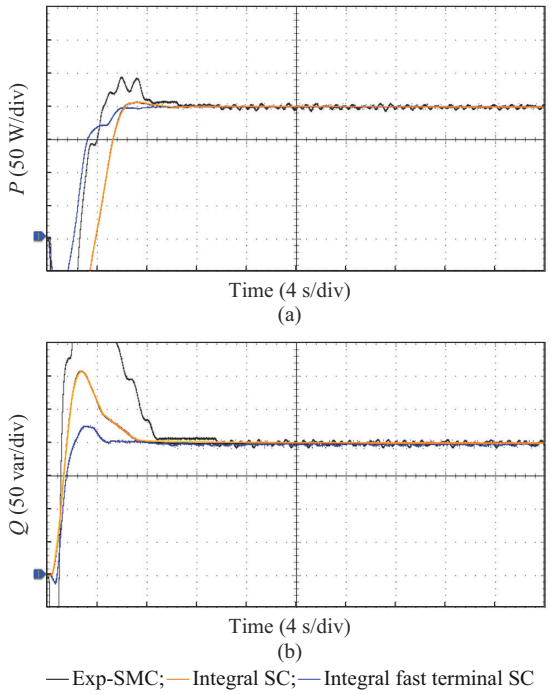

Fig. 11. Experimental results for transient performances of integral fast terminal SC, integral SC, and power-rate exponential SMC. (a) Active power. (b) Reactive power.

TABLE VI
EXPERIMENTAL QUANTITATIVE COMPARISON OF INTEGRAL FAST TERMINAL SC, INTEGRAL SC, AND POWER-RATE EXPONENTIAL SMC

Performance	Controller	The 1st over shoot (%)	Transient time (s)	Error	Chattering
Active power	Integral fast terminal SC	0	0.5	0	Free
	Integral SC	5	0.9	0	Free
	Power-rate exponential SMC	25	0.8	0	Small
Reactive power	Integral fast terminal SC	15	0.5	0	Free
	Integral SC	50	0.8	0	Free
	Power-rate exponential SMC	100	1.4	0	Small

VI. CONCLUSION

This paper presents an effective control scheme for the injected current of the inverters in DGSs or microgrids. The proposed control scheme is based on two proposed versions of SC. The first version is integral SC, and the second is integral fast terminal SC. The macro-variable functions of both versions have an integral term to guarantee zero steady-state error. The simulation results demonstrate that the integral fast terminal SC is slightly faster than integral SC.More importantly, the comparison results demonstrate that the proposed SC schemes are chattering-free with fewer controller parameters for tuning and a better dynamic performance of the injected currents. The experimental results validate the superior performance of the proposed SC schemes compared with power-rate exponential SMC considering the chattering and dynamic performances.

APPENDIX A

A. Stability Proof of Integral SC

This proof starts with defining its Lyapunov equation as Euclidean norm of macro-variable function, which is given as:

$$V(\psi)=\frac{1}{2}\psi^2(e)=\frac{1}{2}\psi(e)\psi(e) \tag{A1}$$

where $\psi^2(e)>0$.

Considering the marco-variable function defined as in (9), the derivative of the Lyapunov equation is written as:

$$\dot{V}(\psi)=\psi(e)\dot{\psi}(e) \tag{A2}$$

$$\begin{cases}\dot{V}(\psi)=\psi(e)(\lambda_I\dot{e}+\lambda_2 e)\\ \dot{x}_I=\dot{e}\end{cases} \tag{A3}$$

$$\dot{V}(\psi)=\psi(e)(\lambda_1\dot{x}_I+\lambda_2 e) \tag{A4}$$

Substituting $\dot{\boldsymbol{x}}$ from its definition in (7) leads to:

$$\dot{V}(\psi)=\psi(\boldsymbol{e})\left[\lambda_1(\boldsymbol{A}\boldsymbol{x}_I+\boldsymbol{B}\boldsymbol{u}+\boldsymbol{F}\boldsymbol{d})+\lambda_2\boldsymbol{e}\right] \tag{A5}$$

Substituting $\boldsymbol{u}$ of (11) in (A5) and simplifying the resultant equations leads to:

$$\dot{V}=\psi(\boldsymbol{e})\lambda_1\boldsymbol{A}\boldsymbol{x}_I+\lambda_1\boldsymbol{B}\left\{-\boldsymbol{B}^{-1}(\boldsymbol{T}\lambda_1)^{-1}\left[(\boldsymbol{T}\lambda_2+\lambda_1)\boldsymbol{e}+\lambda_2\int\boldsymbol{e}\,\mathrm{d}t\right]+\boldsymbol{A}\boldsymbol{x}_I+\boldsymbol{F}\boldsymbol{d}\right\}+\lambda_1\boldsymbol{F}\boldsymbol{d}+\lambda_2\boldsymbol{e}\Rightarrow$$

$$\dot{V}=\psi(\boldsymbol{e})\left(\lambda_1\boldsymbol{A}\boldsymbol{x}_I-\lambda_1\boldsymbol{B}\boldsymbol{B}^{-1}\lambda_1^{-1}\boldsymbol{T}^{-1}\boldsymbol{T}\lambda_2\boldsymbol{e}-\lambda_1\boldsymbol{B}\boldsymbol{B}^{-1}\lambda_1^{-1}\boldsymbol{T}^{-1}\lambda_1\boldsymbol{e}-\lambda_1\cdot\boldsymbol{B}\boldsymbol{B}^{-1}\lambda_1^{-1}\boldsymbol{T}^{-1}\lambda_2\int\boldsymbol{e}\mathrm{d}t-\lambda_1\boldsymbol{B}\boldsymbol{B}^{-1}\boldsymbol{A}\boldsymbol{x}_I-\lambda_1\boldsymbol{B}\boldsymbol{B}^{-1}\boldsymbol{F}\boldsymbol{d}\lambda_1\boldsymbol{F}\boldsymbol{d}+\lambda_2\boldsymbol{e}\right) \tag{A6}$$

where $\boldsymbol{T}$ and $\boldsymbol{T}^{-1}$ are the positive definite diagonal matrices, and $\boldsymbol{T}^{-1}>\boldsymbol{0}$.

After some mathematical simplifications, (A6) is rewritten as:

$$\dot{V}(\psi)=\psi(\boldsymbol{e})\left(-\boldsymbol{T}^{-1}\lambda_1\boldsymbol{e}-\boldsymbol{T}^{-1}\lambda_2\int\boldsymbol{e}\mathrm{d}t\right) \tag{A7}$$

$$\dot{V}(\psi)=\psi(\boldsymbol{e})(-\boldsymbol{T}^{-1})\left(\lambda_1\boldsymbol{e}+\lambda_2\int\boldsymbol{e}\mathrm{d}t\right) \tag{A8}$$

$$\begin{cases}\dot{V}(\psi)=-\psi(\boldsymbol{e})\boldsymbol{T}^{-1}\psi(\boldsymbol{e})\\ \dot{V}(\psi)=-\boldsymbol{T}^{-1}\psi^2(\boldsymbol{e})\\ \dot{V}(\psi)<\boldsymbol{0}\end{cases} \tag{A9}$$

The time derivative of Lyapunov equation $\dot{V}(\psi)$ in (A9) is always negative, then the system with the suggested scheme is stable for all values of $\psi(\boldsymbol{e})$.

B. Stability Proof of Integral Fast Terminal SC

The Lypunouv function for the integral fast terminal SC is defined as:

$$V(\psi)=\frac{1}{2}\psi^2(\boldsymbol{e})=\frac{1}{2}\psi(\boldsymbol{e})\psi(\boldsymbol{e}) \tag{A10}$$

Considering the marco-varibale function as defined in (12), the derivative of the Lyapunov equation is written as:

$$\dot{V}(\psi)=\psi(\boldsymbol{e})\dot{\psi}(\boldsymbol{e}) \tag{A11}$$

$$\dot{V}(\psi)=\psi(\boldsymbol{e})\left(\lambda_1\frac{\mathrm{d}}{\mathrm{d}t}\boldsymbol{e}^{\frac{a}{b}}+\lambda_2\dot{\boldsymbol{e}}+\lambda_3\boldsymbol{e}\right)\Rightarrow\dot{V}(\psi)=\psi(\boldsymbol{e})\left[\lambda_1\frac{\mathrm{d}}{\mathrm{d}t}\boldsymbol{e}^{\frac{a}{b}}+\lambda_2(\boldsymbol{A}\boldsymbol{x}_I+\boldsymbol{B}\boldsymbol{u}+\boldsymbol{F}\boldsymbol{d})+\lambda_3\boldsymbol{e}\right] \tag{A12}$$

where $\dot{\boldsymbol{x}}_I=\dot{\boldsymbol{e}}$.

Substituting $\boldsymbol{u}$ of (13) in (A12) yields:

$$\dot{V}=\psi(\boldsymbol{e})\left\{\lambda_1\frac{\mathrm{d}}{\mathrm{d}t}\boldsymbol{e}^{\frac{p}{q}}+\lambda_2\boldsymbol{A}\boldsymbol{x}_I+\lambda_2\boldsymbol{F}\boldsymbol{d}+\lambda_3\boldsymbol{e}-\lambda_2\boldsymbol{B}\left[\boldsymbol{B}^{-1}\left((\boldsymbol{T}\lambda_2)^{-1}\cdot\left(\left(\boldsymbol{T}\lambda_1\frac{\mathrm{d}}{\mathrm{d}t}+\lambda_1\right)\boldsymbol{e}^{\frac{a}{b}}+(\boldsymbol{T}\lambda_3+\lambda_2)\boldsymbol{e}\right)+\lambda_3\int\boldsymbol{e}\mathrm{d}t\right)+\boldsymbol{A}\boldsymbol{x}_I+\boldsymbol{F}\boldsymbol{d}\right]\right\} \tag{A13}$$

Based on some mathematical simplifications, (A13) is rewritten as:

$$\dot{V}=\psi(\boldsymbol{e})\left(\lambda_1\frac{\mathrm{d}}{\mathrm{d}t}\boldsymbol{e}^{\frac{a}{b}}+\lambda_2\boldsymbol{A}\boldsymbol{x}+\lambda_2\boldsymbol{F}\boldsymbol{d}+\lambda_3\boldsymbol{e}-\lambda_2\boldsymbol{B}\boldsymbol{B}^{-1}\lambda_2^{-1}\boldsymbol{T}^{-1}\boldsymbol{T}\lambda_1-\frac{\mathrm{d}}{\mathrm{d}t}\boldsymbol{e}^{\frac{a}{b}}-\lambda_2\boldsymbol{B}\boldsymbol{B}^{-1}\lambda_2^{-1}\boldsymbol{T}^{-1}\lambda_1\boldsymbol{e}^{\frac{a}{b}}-\lambda_2\boldsymbol{B}\boldsymbol{B}^{-1}\lambda_2^{-1}\boldsymbol{T}^{-1}\boldsymbol{T}\lambda_3\boldsymbol{e}-\lambda_2\boldsymbol{B}\boldsymbol{B}^{-1}\lambda_2^{-1}\boldsymbol{T}^{-1}\lambda_2\boldsymbol{e}-\lambda_2\boldsymbol{B}\boldsymbol{B}^{-1}\lambda_2^{-1}\boldsymbol{T}^{-1}\lambda_3\int\boldsymbol{e}\mathrm{d}t-\lambda_2\boldsymbol{B}\boldsymbol{B}^{-1}\boldsymbol{A}\boldsymbol{x}_I-\lambda_2\boldsymbol{B}\boldsymbol{B}^{-1}\boldsymbol{F}\boldsymbol{d}\right) \tag{A14}$$

The simplification of (A14) leads to:

$$\dot{V}(\psi)=\psi(\boldsymbol{e})(-\boldsymbol{T}^{-1})\left(\lambda_1\boldsymbol{e}^{\frac{a}{b}}+\lambda_2\boldsymbol{e}+\lambda_3\int\boldsymbol{e}\mathrm{d}t\right) \tag{A15}$$

$$\begin{cases}\dot{V}(\psi)=-\psi(\boldsymbol{e})\boldsymbol{T}^{-1}\psi(\boldsymbol{e})\\ \dot{V}(\psi)=-\boldsymbol{T}^{-1}\psi^2(\boldsymbol{e})\\ \dot{V}(\psi)<\boldsymbol{0}\end{cases} \tag{A16}$$

Then the system with its suggested scheme is always stable for all values of $\psi(\boldsymbol{e})$.

APPENDIX B

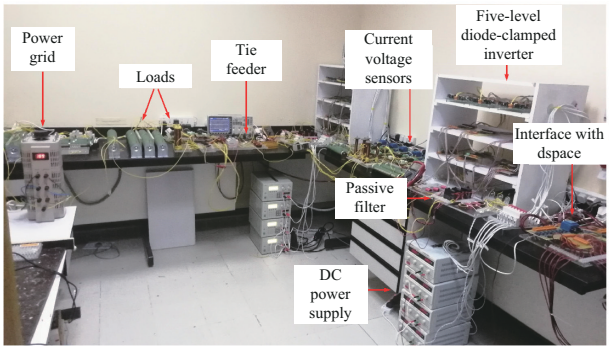

Fig. B1. Experimental setup.

REFERENCES

[1] *IEEE Standard for Interconnection and Interoperability of Distributed Energy Resources with Associated Electric Power Systems Interfaces*, IEEE 1547-2018.

[2] G. Pepermansa, J. Driesenb, D. Haeseldonckxc *et al*., "Distributed generation: definition, benefits and issues," *International Journal on Energy Policy*, vol. 33, no. 6, pp. 787-798, Apr. 2005.

[3] T. Ackermann, G. Andersson, and L. Soder, "Distributed generation: a definition," *Journal of Electric Power System Research-Elsevier*, vol. 57, no. 3, pp. 195-204, Apr. 2001.

[4] Z. A. Arfeen, A. B. Khairuddin, R. M. Larik *et al*., "Control of distributed generation systems for microgrid applications: a technological review," *International Transactions on Electrical Energy Systems*, vol. 29, no. 9, pp. 1-26, Sept. 2019.

[5] Y. I. Mohamed, H. H. Zeineldin, M. M. A. Salama *et al*., "Seamless formation and robust control of distributed generation microgrids via direct voltage control and optimized dynamic power sharing," *IEEE Transactions on Power Electronics*, vol. 27, no. 3, pp. 1282-1293, Mar. 2012.

[6] A. M. Bouzid, J. M. Guerrero, A. Cheriti *et al*., "A survey on control of electric power distributed generation systems for microgrid applications," *Renewable and Sustainable Energy Reviews*, vol. 44, pp. 751-766, Apr. 2015.

[7] X. Wang, X. Ruan, C. Bao *et al*., "Design of the PI regulator and feedback coefficient of capacitor current for grid-connected inverter with an LCL filter in discrete-time domain," in *Proceedings of IEEE Energy Conversion Congress and Exposition (ECCE)*, Raleigh, USA, Sept.

2012, pp. 1657-1662.
[8] J. G. Hwang, P. W. Lehn, and M. Winkelnkemper, "A generalized class of stationary frame-current controllers for grid-connected inverter," *IEEE Transactions on Power Delivery*, vol. 25, no. 4, pp. 2742-2751, Oct. 2010.
[9] L. Shang and J. Hu, "Sliding-mode-based direct power control of grid-connected wind-turbine-driven doubly fed induction generators under unbalanced grid voltage conditions," *IEEE Transactions on Energy Convergence*, vol. 27, no. 2, pp. 362-374, Jun. 2012.
[10] J. Hu and B. Hu, "Direct active and reactive power regulation of grid connected voltage source converters using sliding mode control approach," in *Proceeding of International Symposium on Industrial Electronics*, Bari, Italy, Jul. 2010, pp. 1-4.
[11] L. Shang, D. Sun, and J. Hu, "Sliding-mode-based direct power control of grid-connected voltage-sourced inverters under unbalanced network conditions," *IET on Power Electronics*, vol. 4, no. 5, pp. 570-579, May 2011.
[12] D. H. Phan and S. Huang, "Super-twisting sliding mode control design of three-phase inverter for microgrid distributed generation systems," *Journal of Control, Automation and Electric Systems*, vol. 26, pp. 179-188, Apr. 2016.
[13] A. Elnady and A. Adam, "Accurate self-adaptive PI controller of direct power and voltage control for distributed generation systems," *International Transactions on Electrical Energy Systems*, vol. 28. No. 10, pp. 1-10, Oct. 2018.
[14] S. Kwak, U.-Chul Moon, and J.-Cheol Park, "Predictive-control-based direct power control with an adaptive parameter identification technique for improved AFE performance," *IEEE Transactions on Power Electronics*, vol. 29, no. 11, pp. 6178-6187, Nov. 2014.
[15] Z. Song, W. Chen, and C. Xia, "Predictive direct power control for three-phase grid-connected converters without sector information and voltage vector selection," *IEEE Transactions on Power Electronics*, vol. 29, no. 10, pp. 5518-5531, Oct. 2014.
[16] R. Teodorescu, F. Blaabjerg, M. Liserre *et al*., "Proportional-resonant controllers and filters for grid-connected voltage-source converters," *IEE Proceedings on Electric Power Applications*, vol. 5, pp. 750-762, Sept. 2006.
[17] F. Huerta, D. Pizarro, S. Cobreces *et al*., "LQG servo controller for the current control of LCL grid-connected voltage-source converters," *IEEE Transactions on Industrial Electronics*, vol. 11, pp. 4272-4284, Nov. 2012.
[18] A. Timbus, "Grid monitoring and advanced control of distributed power generation systems," Ph.D. dissertation, Institute of Energy Technology, Aalborg University, Aalborg, Denmark, 2007.
[19] M. Mahmud, H. Pota, and M. Hossain, "Nonlinear controller design for single-phase grid-connected photovoltaic systems using partial feedback linearization," in *Proceedings of the 2012 Australian Control Conference-Engineers Australia*, Sydney, Australia, Nov. 2012, pp. 30-36.
[20] Q. Zhong and T. Hornik, "Cascaded current-voltage control to improve the power quality for a grid-connected inverter with a local load," *IEEE Transactions on Industrial Electronics*, vol. 60, no. 4, pp. 344-1355, Apr. 2013.
[21] M. Abu-sara and S. Sharkh, "Design of a robust digital current controller for a grid connected interleaved inverter," in *Proceedings of IEEE International Symposium on Industrial Electronics*, Bari, Italy, Jul. 2010, pp. 3-6.
[22] J. Qian, K. Li, H. Wu *et al*., "Synergetic control of grid-connected photovoltaic systems," *International Journal of Photoenergy*, vol. 2017, pp. 1-11, Mar. 2017.
[23] M. Suleiman, A. Elnady, and A. Osman, "Experimental verification for improved phase-disposition PWM of three-phase five-level diode-clamped inverter," *International Journal of Circuit Theory and Applications*, vol. 49, no. 6, pp. 1828-1848, Feb. 2021.
[24] A. A. Kolesnikov and G. E. Veselov, *Modern Applied Control Theory*: *Synergetic Approach in Control Theory*. Taganrog: TSURE Press, 2000.
[25] A. Kolesnikov, G. Veselov, A. Monti *et al*., "Synergetic synthesis of DC-DC boost converter controllers: theory and experimental analysis," in *Proceedings of APEC Seventeenth Annual IEEE Applied Power Electronics Conference and Exposition*, Dallas, USA, Mar. 2002, pp. 409-415.
[26] D. Li, K. Proddutur, E. Santi *et al*., "SC of a boost converter: theory and experimental verification," in *Proceedings of IEEE Southeast Conference 2002*, Columbia, USA, Apr. 2002, pp. 197-200.
[27] Z. Yu, Q. Ai, J. Gong *et al*., "A novel secondary control for microgrid based on SC of multi-agent system," *Energies*, vol. 9, no. 4, pp. 243-253, Mar. 2016.
[28] H. Komurcugil, "Adaptive terminal sliding-mode control strategy for DC-DC converter," *ISA Transactions*, vol. 51, no. 6, pp. 673-681, Nov. 2012.
[29] A. Ahifar, A. R. Noee, and Z. Rahmani, "Terminal synergetic design of a nonlinear robot manipulator in the presence of disturbances," *International Journal for Computation and Mathematics in Electrical and Electronic Engineering*, vol. 37, no. 7, pp. 1-12, Jan. 2018.
[30] H. Abderrezek and M. N. Harmas, "Particle swarm optimization of a terminal synergetic controllers for a DC-DC converter," *International Journal of Industrial and Manufacturing Engineering*, vol. 8, no. 8, pp. 1248-1255, Dec. 2014.
[31] S. Xu, C. Chen, and Z. Wu, "Study of nonsingular fast-terminal sliding-mode fault-tolerant control," *IEEE Transactions on Industrial Electronics*, vol. 62, no. 6, pp. 3906-3913, Feb. 2015.
[32] E. Santi, A. Monti, D. Li *et al*., "Synergetic control for DC-DC boost converter: implementation options," *IEEE Transactions on Industrial Electronics*, vol. 39, no. 6, pp. 1803-1813, Dec. 2003.
[33] V. Utkin and J. Shi, "Integral sliding mode in systems operating under uncertainty conditions," in *Proceedings of 35th IEEE Conference on Decision and Control*, Kobe, Japan, Dec. 1996, pp. 4591-4596.
[34] A. Elnady, A. Noureldin, and A. A. Adam, "Integral terminal synergetic based direct power control for distributed generation systems," *IEEE Transactions on Smart Grids*, vol. 13, no. 2, pp. 1287-1297, Mar. 2022.
[35] N. Zerrouga, M. N. Harmasa, S. Benaggouneb *et al*., "DSP-based implementation of fast-terminal synergetic control for a DC-DC Buck converter," *Journal of the Franklin Institute*, vol. 355, no. 5, pp. 2329-2343, Mar. 2018.
[36] A. Elnady and M. Alshabi, "Advanced exponential sliding mode control for microgrid at autonomous and grid-connected modes," *Bulletins of Electrical Engineering and Informatics*, vol. 10, no. 1, pp. 474-486, Feb. 2021.
[37] C. Fallaha, M. Saad, H. Y. Kanaan *et al*., "Sliding mode robot control with exponential reaching law," *IEEE Transactions on Industrial Electronics*, vol. 52, no. 2, pp. 600-610, Feb. 2011.

A. Elnady received the bachelor's degree from Department of Electric Power and Machines, Faculty of Engineering, Cairo University, Cairo, Egypt, in 1994, where he also received the Master degree in Electric Power Engineering, in 1998. He received the Ph.D. degree from Electrical and Computer Engineering, Faculty of Engineering, University of Waterloo, Waterloo, Canada, in 2004. His research interests include power-electronics applications in drive systems and distribution systems, integration of renewable energy resources into power grids, distributed generation systems, microgrids, and smart girds.

A. Noureldin received the B.Sc. degree in electrical engineering and the M. Sc. degree in engineering physics both from Cairo University, Cairo, Egypt, in 1993 and 1998, respectively. In addition, he received the Ph.D. degree in electrical and computer engineering from The University of Calgary, Alberta, Canada, in 2002. He is a Senior Member of IEEE and a Professional Member of the Institute of Navigation (ION), Manassas, USA. He published two books, 4 book chapters and over 270 papers in academic journals, conference, and workshop proceedings, in which he received several awards. He is a Professor at the Department of Electrical and Computer Engineering, Royal Military College of Canada (RMCC) with Cross-Appointment at both the School of Computing and the Department of Electrical and Computer Engineering, Queen's University, Kingston, Ontario, Canada. His research interests include wireless positioning and localization, multi-sensor fusion for positioning and navigation, machine vision, vehicular, Internet of Things (IoT), machine intelligence, and deep learning.

A. A. Adam received the B.Sc. degree in electrical engineering from Khartoum University, Khartoum, Sudan, in 1991, the M. Sc. degree in electrical engineering from University of Bagdad, Bagdad, Iraq, in 1997, and the Ph. D. degree in electrical engineering from Technical University of Yildiz, Istanbul, Turkey, in 2007. His research interests include control of electrical machines and drives, power electronics applications, and dynamics of electrical power system.